Mediterranean Journal of Basic and Applied Sciences (MJBAS)
Volume 7, Issue 1, Pages 154-166, January-March 2023

Detecting Cardio-Vascular Acoustics in an Incipient Turbulence

Francis E. Nzerem[1*] & Orumie Ukamaka Cynthia[2]

[1,2]*Department of Mathematics and Statistics, University of Port Harcourt, Choba. Email: frankjournals@yahoo.com**

DOI: https://doi.org/10.46382/MJBAS.2023.7113

Article Received: 07 February 2023 *Article Accepted: 22 March 2023* *Article Published: 30 March 2023*

ABSTRACT

Cardiovascular flow maintains the integrity of animated life, especially of humans. This flow goes fuzzy in the event of turbulence. In pathological states, vascular stenosis is usually the culprit in turbulence. Whether turbulence ensues from a physiological state or else, there must be a concomitant sound that is at variance with the normative flow acoustics. This sound emanates from a source point which is more or less within the inception of stenosis. This paper aims to identify the vascular sound field that emanates from a source point, maybe, due to stenosis. As a prelude, it furnished the windowed equations of motion for a fluid (blood) occupying a vascular region to derive the fluid density form of the acoustic analogy. However, the parameter of higher interest in vascular acoustics is turbulent pressure. So, it was well considered, and its relationship with acceleration at the monitor points on the aortic surface was supplied. An aspect of this work is the analysis of heart murmur. The heart was presumed here to admit Kelvin-Voigt's viscoelastic model and, therefore, the equations governing the model hold well in the present case. Details here suggest that the hemodynamic pressure fluctuation on the aortic lumen boundary and the concomitant turbulent flow precipitates aortic stenosis murmur.

Keywords: Fluctuations; Stenosis; Coherent perturbations; Reynolds stress; Murmurs; Signals; Fourier/Wavelet transform.

1. Introduction

Auditory physiognomies have been used to localise stenosis in numerous vessels. The non-invasive diagnostic technique, if achievable, seems a better approach to the detection of cardiovascular anomalies. This was echoed by Akay et al. [1], sought by Lees and Kistler [2] and Miller *et al*. [3] who used the spectral analysis technique for the detection of bruits in the carotid artery. Noticeable diastolic murmurs have also been recorded in patients with coronary artery stenosis [4, 5, 6]. Interestingly, Wang *et al.* [4] reported that acoustic quantities acquired from sensitive microphones placed on the chest are being used in a procedure for a non-invasive diagnosis of coronary artery disease (CAD). Moreover, the spectral content of isolated diastolic heart sounds has been estimated by using exclusively developed signal processing techniques. The result indicates a rise in high-frequency components in patients with occlusive coronary arteries. Studies showed that turbulent blood flow generates sounds in partially occluded arteries in the event of coronary stenosis [7, 8**].** In a physiological state, blood flow is largely laminar. Typically, the laminar flow may be disturbed and transit to turbulence mediated by high flow velocity in which the critical Reynolds number (Re) is exceeded. Thus, the blood flow may well be described as being chaotic as it does not flow linearly and smoothly in adjacent layers. It is pertinent to note that transient turbulent flow also applies to the physiological state, as may be observed in many postural maneuvres.

In the cardiovascular system the vibrating structures, distressed regions of turbulent flow, mixing of flows of diverse temperatures, and their semblances produce large pressure fluctuations that are transferred through a fluid as sound. The turbulent intensities can be relatively large between the stenosis (where prevalent) and the region where turbulence has considerably decayed, and the wall of the artery can be subjected to large fluctuating stresses imposed by the turbulent flow. Turbulence is marked by the recurrent unexpected changes in the flow pattern which transcends the understanding of the instantaneous motions. The instantaneous fluid velocity induces convection which is arguably the cardinal process in turbulent flows. Since molecular diffusion does not give an

inspiring contribution to spatial transport at a high Reynolds number, convection mediates the transference of momentum, chemical species, and enthalpy [9]. Sometimes a statistical description of turbulence which comprises a probability distribution for stationary flows to determine the nature of turbulent velocity fluctuations holds well for the description of turbulent motion [10]. Monin and Yaglom [11] articulated the velocity structure functions (VSF) which are directly related to the probability density function (PDF) of the local dissipation rate. It is therefore a pertinent descriptor of the PDF of the dissipation rate which completely describes the statistics of turbulent velocity when considerations are on the Eulerian/Lagrangian fluid particle velocity framework.

The incidence of turbulence is felt at various segments of the cardiovascular system. In the ascending aorta, the laminar flow may transit to turbulent in the event of extremely high flow velocity [12] which is marked by intra-arterial ejection murmurs [13]. The coronary arterial blood flow is maximum during diastole, and the murmurs induced by turbulent blood flow through partially occluded (stenosed) coronary arteries are most audible [1]. Fredberg [14] investigated two major descriptors of the fluctuating turbulent pressure at the wall: the root-mean-square pressure and the spectral density of pressure. Elsewhere [15] the spectral analysis techniques for blood flow velocity were detailed.

In this work, we sought a turbulent pressure source point; we regard a single point source in the arterial compartment as a source whose dimensions are much less than the wavelength of sound generated. It is to be accepted, however, that a random point source is an avid approximation since the lengths of vascular vessels may be considered 'short'. Details concerning turbulent fields in short vessels are sparse. The identification of the source point would aid in localizing vascular sounds. The hemodynamic pressure fluctuation on the aortic lumen boundary was discussed. It is a factor in the turbulent flow that is often implicated in the creation of aortic stenosis murmur.

2. Fully developed pipe flow

Fully-developed flow describes the case in which the velocity profile is invariant along the direction of flow (in the axial direction). Thus, two different axial locations in the pipe manifest the same velocity profile. Laufer [16] investigated the structure of turbulence in fully developed pipe flow. Consider a cylindrical pipe analogous to the arterial/venous configuration.

2.1. Perturbation equations in cylindrical coordinates

Considering a section of the pipe governed by incompressible mean flow, the continuity equation and Reynolds equation in cylindrical polar coordinates may be furnished by Reynolds equations of pipe flow [16, 9]. Using the basic Navier-Stokes equations the perturbation equation of continuity reads:

$$\frac{\partial \tilde{\rho}}{\partial t} + \bar{u}_i \frac{\partial \tilde{\rho}}{\partial x_i} + \rho_0 \frac{\partial \tilde{u}_i}{\partial x_i} = 0, \qquad (1)$$

where ρ is the fluid density, and u_i is the velocity. The momentum equation for the coherent perturbations is of the form**:**

$$\left(\frac{\partial \tilde{u}_i}{\partial t}+\tilde{u}_j\frac{\partial \bar{u}_i}{\partial x_j}+\bar{u}_j\frac{\partial \tilde{u}_i}{\partial x_j}+\frac{\tilde{\rho}\bar{u}_j}{\rho_0}\frac{\partial \bar{u}_i}{\partial x_j}\right)=-\frac{1}{\rho_0}\frac{\partial \tilde{p}}{\partial x_i}+\nu\left[\frac{\partial^2 \tilde{u}_i}{\partial x_j\partial x_j}+\left(\frac{1}{3}+\frac{\mu_B}{\mu}\right)\frac{\partial^2 \tilde{u}_j}{\partial x_j\partial x_i}\right]-\frac{\partial \tilde{\mathrm{r}}_{ij}}{\partial x_j}, \qquad (2)$$

where μ is the dynamic viscosity, and μ_B is the bulk viscosity (see Pierce [17]) which is assumed constant here. The perturbation Reynolds stress reads:

$$\tilde{\mathrm{r}}_{ij}\equiv\left\langle u_i'u_j'\right\rangle-\overline{u_i'u_j'}. \qquad (3)$$

From Carey [18], the quantity $\tilde{\mathrm{r}}_{ij}$ may be understood as the oscillation of the background Reynolds stresses due to the passage of the coherent perturbations. Equations (2, 3) describe the motion of a Newtonian fluid, accompanied by the motion of coherent perturbations, for example, sound wave propagation. In the treatment of cardiovascular flows, it is frequently desirable to scrutinize the flow and the coherent perturbation quantities separately, basically by some splitting technique (see Morfey [19]). The following decomposition ensues:

$$W(\mathrm{x},t)=\bar{W}(\mathrm{x})+\tilde{W}(\mathrm{x},t)+\hat{W}(\mathrm{x},t), \qquad (4)$$

where $\bar{W}$ encodes the mean (time-averaged) contribution, $\tilde{W}$ is the periodic wave (coherent perturbation) driven by the pulsatile structure of the flow, and $\hat{W}$ signifies the turbulent fluctuation. Now, W indicates any one of the variables: ρ, u_i, T, or p, as the case requires. We define $\bar{W}(\mathrm{x},\mathrm{t})$ as

$$\bar{W}(\mathrm{x},\mathrm{t})=\lim_{\varepsilon\to\infty}\frac{1}{\varepsilon}\int_t^{t+\varepsilon}W(\mathrm{x},\mathrm{t}')\mathrm{d}t', \qquad (5)$$

and the phase average is

$$\left\langle W(\mathrm{x},t)\right\rangle=\lim_{N\to\infty}\frac{1}{N_p}\sum_{\xi=0}^{N_p}W\left(\mathrm{x},\,t+\frac{\beta}{f}\right), \qquad (6)$$

where f signifies the frequency of the coherent perturbation.

A fully developed turbulent pipe flow is characterised by a homogeneous stream-wise mean flow with the velocity, $\bar{\boldsymbol{u}}=[\,\bar{u}_x(r),\,0,\,0]$, which is locally parallel. So, $\bar{\boldsymbol{u}}=[\,\bar{u}_x(r),\,0,\,0]$ is parallel to the x-axis and fluctuates in the radial direction r. The perturbation equations in cylindrical coordinates are:

$$\left(\frac{\partial}{\partial t}+\bar{\vartheta}\right)\frac{\tilde{\rho}}{\rho_0}+\left(\frac{\partial \tilde{u}_r}{\partial r}+\frac{\tilde{u}_r}{r}+\frac{1}{r}\frac{\partial \tilde{u}_\theta}{\partial \theta}+\frac{\partial \tilde{u}_x}{\partial x}\right)=0 \qquad (\textit{continuity equation}) \qquad (7)$$

$$\begin{aligned}\left(\frac{\partial}{\partial t}+\bar{\vartheta}\right)\tilde{u}_x+\frac{\tilde{\rho}}{\rho_0}\bar{\vartheta}\bar{u}_x=&-\frac{1}{\rho_0}\frac{\partial \tilde{\rho}}{\partial x}+\nu\left(\frac{\partial^2 \tilde{u}_x}{\partial r^2}+\frac{1}{r}\frac{\partial \tilde{u}_x}{\partial r}+\frac{1}{r^2}\frac{\partial^2 \tilde{u}_x}{\partial \theta^2}+\frac{\partial^2 \tilde{u}_x}{\partial x^2}\right)\\&+\nu\left(\frac{1}{3}+\frac{\mu_B}{\mu}\right)\left(\frac{\partial^2 \tilde{u}_r}{\partial x\partial r}+\frac{1}{r}\frac{\partial^2 \tilde{u}_\theta}{\partial x\partial \theta}+\frac{1}{r}\frac{\partial^2 \tilde{u}_r}{\partial x}+\frac{\partial^2 \tilde{u}_x}{\partial x^2}\right)\\&-\left[\frac{\partial \tilde{r}_{rx}}{\partial r}+\frac{1}{r}\left(\frac{\partial \tilde{r}_{\theta x}}{\partial \theta}+\tilde{r}_{rx}\right)+\frac{\partial \tilde{r}_{xx}}{\partial x}\right]\end{aligned} \qquad (\text{x}-\text{momentum equation}) \qquad (8)$$

Mediterranean Journal of Basic and Applied Sciences (MJBAS)
Volume 7, Issue 1, Pages 154-166, January-March 2023

$$\left(\frac{\partial}{\partial t}+\bar{\vartheta}\right)\tilde{u}_r+\frac{\tilde{\rho}}{\rho_0}\bar{\vartheta}\bar{u}_r-2\frac{\bar{u}_\theta\tilde{u}_\theta}{r}=-\frac{1}{\rho_0}\frac{\partial\tilde{\rho}}{\partial r}+\nu\left(\frac{\partial^2\tilde{u}_r}{\partial r^2}+\frac{1}{r^2}\frac{\partial^2\tilde{u}_r}{\partial\theta^2}+\frac{1}{r}\frac{\partial\tilde{u}_r}{\partial r}-\frac{\tilde{u}_r}{r^2}-\frac{2}{r^2}\frac{\partial\tilde{u}_\theta}{\partial\theta}+\frac{\partial^2\tilde{u}_r}{\partial x^2}\right)$$
$$+\nu\left(\frac{1}{3}+\frac{\mu_B}{\mu}\right)\left(\frac{\partial^2\tilde{u}_r}{\partial r^2}+\frac{1}{r}\frac{\partial^2\tilde{u}_\theta}{\partial\theta\partial r}+\frac{1}{r}\frac{\partial^2\tilde{u}_r}{\partial r}-\frac{1}{r^2}\frac{\partial\tilde{u}_\theta}{\partial\theta}-\frac{\tilde{u}_r}{r^2}+\frac{\partial^2\tilde{u}_x}{\partial r\partial x}\right)$$
$$-\left[\frac{\partial\tilde{r}_{rr}}{\partial r}+\frac{1}{r}\left(\frac{\partial\tilde{r}_{\theta x}}{\partial\theta}+(\tilde{r}_{rr}-\tilde{r}_{\theta\theta})\right)+\frac{\partial\tilde{r}_{xr}}{\partial x}\right] \quad (r-\textit{momentum equation}) \qquad (9)$$

$$\left(\frac{\partial}{\partial t}+\bar{\vartheta}+\frac{\bar{u}_r}{r}\right)\tilde{u}_\theta+\left(\frac{\tilde{\rho}}{\rho_0}\bar{\varsigma}+\frac{\tilde{u}_r}{r}\right)\bar{u}_\theta=-\frac{1}{\rho_0 r}\frac{\partial\tilde{\rho}}{\partial\theta}+\nu\left(\frac{\partial^2\tilde{u}_\theta}{\partial r^2}+\frac{1}{r}\frac{\partial\tilde{u}_\theta}{\partial r}-\frac{\tilde{u}_\theta}{r^2}+\frac{1}{r^2}\frac{\partial}{\partial\theta}\left(\frac{\partial\tilde{u}_\theta}{\partial\theta}+2\tilde{u}_r\right)+\frac{\partial^2\tilde{u}_\theta}{\partial x^2}\right)$$
$$+\nu\left(\frac{1}{3}+\frac{\mu_B}{\mu}\right)\left(\frac{1}{r}\frac{\partial^2\tilde{u}_r}{\partial\theta\partial r}+\frac{1}{r^2}\frac{\partial}{\partial\theta}\left(\tilde{u}_r+\frac{\partial\tilde{u}_\theta}{\partial\theta}\right)+\frac{1}{r}\frac{\partial^2\tilde{u}_x}{\partial x\partial\theta}\right)$$
$$-\left[\frac{\partial\tilde{r}_{r\theta}}{\partial r}+\frac{1}{r}\left(\frac{\partial\tilde{r}_{\theta\theta}}{\partial\theta}+(\tilde{r}_{r\theta}-\tilde{r}_{\theta r})\right)+\frac{\partial\tilde{r}_{x\theta}}{\partial x}\right] \quad (\theta-\textit{momentum equation}) \qquad (10)$$

$$\left(\frac{\partial}{\partial t}+\bar{\vartheta}\right)\tilde{T}+\frac{\tilde{\rho}}{\rho_0}\bar{\vartheta}\bar{T}=\frac{1}{c_{p\rho_0}}\left[\left(\frac{\partial}{\partial t}+\bar{\vartheta}\right)\tilde{p}+\tilde{\zeta}\,\bar{p}\right]+\lambda\left(\frac{\partial^2\tilde{T}}{\partial r^2}+\frac{1}{r}\frac{\partial\tilde{T}}{\partial r}+\frac{1}{r^2}\frac{\partial^2\tilde{T}}{\partial\theta^2}+\frac{\partial^2\tilde{T}}{\partial x^2}\right),$$
$$-\left[\frac{\partial\tilde{q}_r}{\partial r}+\frac{1}{r}\left(\frac{\partial\tilde{q}_\theta}{\partial\theta}+\tilde{q}_r\right)+\frac{\partial\tilde{q}_x}{\partial x}\right]+\frac{2\nu}{c_p}(\alpha+\beta) \quad (\textit{The energy equation}) \qquad (11)$$

where,

$\bar{\eta}=\bar{u}_x\frac{\partial}{\partial x}$ and $\tilde{\zeta}=\tilde{u}_x\frac{\partial}{\partial x}$, and $\alpha=\frac{\partial\bar{u}_x}{\partial r}\frac{\partial\tilde{u}_x}{\partial r}$, $\beta=\frac{\partial\bar{u}_x}{\partial r}\frac{\partial\tilde{u}_r}{\partial x}$.

3. Flow in Stenosed Arteries

In the course of systole, blood immediately proximal to a stenosis undergoes laminar flow and experiences convective acceleration as it passes from the intact portion of the artery through the converging section of the stenosis. At a reasonably high Reynolds number, the flow through the diverging section of the stenosis split up from the walls owing to its inability to overcome the adversative pressure gradient. A shear layer susceptible to fluid-dynamical fluxes is created at the frontier between the separated high-velocity jet and the rather slow-moving fluid in the recirculating separation zone. The shear layer created delivers a source from which these instabilities derive energy from the mean flow [14, 20, 21]. This energy extraction process ensues at an amply rapid rate that the instabilities break down into fully turbulent motion before the end of systole if the jet Reynolds number is sufficiently high. As soon as the jet fills the artery, the turbulence begins to evanesce as it could no longer extract energy from the mean flow. The turbulent intensities may be reasonably large within the stenosis and the region where turbulence has considerably decayed. Consequently, the conducting arterial segment may be exposed to enormous fluctuating stresses due to the turbulent flow [14].

3.1. Noise (sound) generation

Noise is a sacrosanct element of turbulence. Acoustic sources which radiate sound develop from velocity and pressure fluctuations. Such sound has varying intensities and directionality that are characteristic of the precise nature and magnitude of the sources and the acoustic features of the adjacent media. Pressure is a factor of interest in the wave equation because ears and the auscultation devices are sensitive to pressure fluctuations. Turbulent fluctuating pressures which are related to acoustical pressure are called *sound pressure* or *sound*, and *intra-arterial sounds* are fluctuations of pressures that are related to sound. [22].

Mediterranean Journal of Basic and Applied Sciences (MJBAS)
Volume 7, Issue 1, Pages 154-166, January-March 2023

Acoustic velocity is commonly used as a boundary condition in computations involving solid bodies. It is the usual fluid dynamic boundary condition that must be satisfied [17]. Thus, a good relationship is found between pressure and velocity. Morfey and Wright [19] formulated bounded domains that enable the application of pressure-based options to the fluid density as a wave variable, thereby refining the pioneering work of Lighthill [23] on acoustic analogy.

The expressions for conservation of mass and momentum of the windowed equations of motion for a fluid occupying a region, *R*., are

$$\overline{\frac{\partial}{\partial t}(\rho-\rho_0)}+\overline{\frac{\partial}{\partial x_i}(\rho u_i)}=0, \qquad \overline{\frac{\partial}{\partial t}(\rho u_i)}+\overline{\frac{\partial}{\partial t}\left(\rho u_i u_j+p_{ij}\right)}=\underline{B_i}. \tag{12}$$

In (12) above and afterward, an overbar implies that the quantity or variable is being multiplied by some Heaviside functions *H* and Ξ; it is windowed in space and time; $p_{ij}=P_{ij}-P_0\delta_{ij}$ where *P* is absolute pressure and P_{ij} is the compressive stress in the fluid; δ_{ij} is the Kronecker delta and B_i is an applied body force per unit volume. The Heaviside functions *H* and Ξ are such that:

$$\mathcal{H}(\boldsymbol{n})=\begin{cases}1 & \text{in } \mathcal{R} \text{ and on } S\\ 0 & \text{in } \mathcal{R}' \text{ (prime denotes complement);}\end{cases} \tag{13}$$

$$\Xi(t)=\begin{cases}1 & \text{for } t\geq 0\\ 0 & \text{for } t<0\end{cases}, \tag{14}$$

In (13), **n** encodes a local normal coordinate described for points in the neighbourhood of *S* and $\boldsymbol{n}=f.\mathbf{S}$ is a moving closed surface in an appropriate dimension, assumed smooth. $|\nabla f|$ is single-valued. The following derivatives apply from the property of the Heaviside function (see Morfey and Wright [19]):

$$\frac{\partial\Xi}{\partial t}=\delta(t), \quad \frac{\partial\Xi}{\partial x_i}=0, \quad \frac{\partial\mathcal{H}}{\partial n}=\delta(n), \quad \frac{\partial\mathcal{H}}{\partial x_i}=\mathbf{n}_i\delta(n), \tag{15}$$

where $\delta(.)$ is the Dirac delta function and $\boldsymbol{n}_i=\partial n/\partial x_i$ is the unit normal to *S*. For any field variable ξ,

$$\overline{\frac{\partial\xi}{\partial x_i}}-\frac{\partial\xi}{\partial x_i}=-\xi\mathbf{n}_i\delta(n)\Xi, \qquad \overline{\frac{\partial\xi}{\partial t}}-\frac{\partial\xi}{\partial t}=\xi\left[v_i\mathbf{n}_i\delta(n)\Xi-\mathcal{H}\delta(t)\right] \tag{16}$$

where $v_i = v\boldsymbol{n}_i$, *v* is the normal velocity of the surface *S* directed into R. Apply equation (16) to equation (12) to get

$$\overline{\frac{\partial}{\partial t}(\rho-\rho_0)}+\frac{\partial}{\partial x_i}\left(\overline{\rho u_i}\right)=(\rho-\rho_0)\mathcal{H}\delta(t)+\left[\rho u_i-(\rho-\rho_0)v_i\right]\mathbf{n}_i\delta(n)\Xi \tag{17}$$

and

$$\frac{\partial}{\partial t}\left(\overline{\rho u_i}\right)+\frac{\partial}{\partial x_i}\left(\overline{\rho u_i u_j+p_{ij}}\right)=\overline{B_i}+\rho u_i\mathcal{H}\delta(t)+\left[\rho u_i\left(u_j-v_j\right)+p_{ij}\right]\mathbf{n}_j\delta(n)\Xi. \tag{18}$$

It is plausible to eliminate $\overline{\rho u_i}$ from (17) and (18) to obtain the second time derivative of the perturbed density valid for all (x_i, *t*). Accordingly,

$$\frac{\partial^2}{\partial t^2}\left(\overline{\rho-\rho_0}\right)=\frac{\partial}{\partial t}[(\rho-\rho_0)\mathcal{H}\delta(t)]-\frac{\partial}{\partial x_i}\left[\rho u_i\mathcal{H}\delta(t)\right]+\frac{\partial}{\partial t}\left[\left[\rho u_i-(\rho-\rho_0)v_i\right]\mathbf{n}_i\delta(n)\Xi\right]$$

$$-\frac{\partial}{\partial x_i}\left[\left[\rho u_i\left(u_j-v_j\right)+p_{ij}\right]\mathbf{n}_j\delta(n)\Xi\right]-\frac{\partial\overline{B_i}}{\partial x_i}+\frac{\partial}{\partial x_i\partial x_j}\left(\overline{\rho u_i u_j+p_{ij}}\right) \quad . \tag{19}$$

The density form of the acoustic analogy reads:

$$\left(\frac{1}{c_0^2}\frac{\partial^2}{\partial t^2}-\nabla^2\right)\left[c_0^2\left(\overline{\rho-\rho_0}\right)\right]=\frac{\partial}{\partial t}\left[(\rho-\rho_0)\mathcal{H}\delta(t)\right]-\frac{\partial}{\partial x_i}\left[\rho u_i\mathcal{H}\delta(t)\right]+\frac{\partial}{\partial t}\left[J_i\mathbf{n}_i\delta(n)\Xi\right] \tag{20}$$
$$-\frac{\partial}{\partial x_i}\left[L_{ij}\mathbf{n}_j\delta(n)\Xi\right]-\frac{\partial\overline{B_i}}{\partial t}+\frac{\partial^2\overline{T_{ij}}}{\partial x_i\partial x_j}$$

T_{ij}, Ji, and L_{ij} on the right of (20) encode:

Lighthill stress tensor

$$T_{ij}=\rho u_i u_j+p_{ij}-c_0^2\left(\rho-\rho_0\right)\delta_{ij}, \tag{21}$$

Surface mass flux vector

$$J_i=\rho u_i-\left(\rho-\rho_0\right)v_i\equiv\rho\left(u_i-v_i\right)+\rho_0 v_i, \tag{22}$$

Surface momentum flux tensor

$$L_{ij}=\rho u_i\left(u_i-v_i\right)+p_{ij}. \tag{23}$$

The right-hand side of (20) represents the sources that characterise the physical properties of the acoustic wave. The first two members are the combined impulsive mass and momentum that drive flow from its original reference state; the second and third members contain Ffowcs Williams & Hawkings (FWH) formulation [22] of surface monopoles and dipoles, demonstrated by Ξ, and subsequently, the volume source terms, with the body force B_i and the stress tensor T_{ij} represented spatially and temporally by H Ξ. Reethuf [24] advocated that mass-flow fluctuations may be associated with monopole sources as compact fluctuating forces, momenta, or pressures in a flow field relate with dipole sources; and fluctuating shear stresses relate with quadrupole sources. The FWH equation (24) with no initial source terms provides an extrapolative bridge between the simulation domain and the acoustic far field. The substitution of the local density ρ by a new variable ρ* related to ρ and making some arithmetic operations give the equation for $\partial^2\left(\overline{\rho^*-\rho_0}\right)/\partial t^2$ in the form (see Reneman *et al.* [25]):

$$\frac{\partial^2\left(\overline{\rho-\rho_0}\right)}{\partial t^2}=\frac{\partial}{\partial t}\left[\left(\rho^*-\rho_0\right)\mathcal{H}\delta(t)\right]-\frac{\partial}{\partial x_i}\left[\rho^* u_i\mathcal{H}\delta(t)\right]+\frac{\partial}{\partial t}\left[\mathrm{J}_i^*\mathbf{n}_i\delta(n)\Xi\right]$$
$$-\frac{\partial}{\partial x_i}\left[L_{ij}^*\mathbf{n}_j\delta(n)\Xi\right]+\frac{\partial\overline{\Psi^*}}{\partial x_i}-\frac{\partial}{\partial x_i}\left[\overline{\Psi^* u_i-(\rho-\rho^*)\frac{Du_i}{Dt}+B_i}\right]+\frac{\partial}{\partial x_i\partial x_j}\left(\overline{\rho^* u_i u_j+p_{ij}}\right) \quad , \tag{24}$$

where J_i^* and L_{ij}^* are similar to J_i and L_{ij} when ρ^* replaces ρ and

$$\Psi^*=\frac{D\rho^*}{Dt}+\rho^*\Delta \quad . \tag{25}$$

A general acoustic analogy now reads:

$$\left(\frac{1}{c_0^2}\frac{\partial^2}{\partial t^2}-\nabla^2\right)\left[c_0^2\left(\overline{\rho^*-\rho_0}\right)\right]=\frac{\partial}{\partial t}\left[(\rho^*-\rho_0)\mathcal{H}\delta(t)\right]-\frac{\partial}{\partial x_i}\left[\rho^* u_i\mathcal{H}\delta(t)\right]+\frac{\partial}{\partial t}\left[J_i^*\boldsymbol{n}_i\delta(n)\Xi\right] \quad (26)$$
$$-\frac{\partial}{\partial x_i}\left[L_{ij}\boldsymbol{n}_j\delta(n)\Xi\right]+\overline{\frac{\partial\Psi^*}{\partial t}}-\frac{\partial}{\partial x_i}\left(\overline{\Psi^* u_i+\frac{\rho^*}{\rho}B_i+\frac{\rho-\rho^*}{\rho}\frac{\partial p_{ij}}{\partial x_j}}\right)+\frac{\partial^2\overline{T_i^*{}_j}}{\partial x_i\partial x_j}$$

where the penultimate term is got by letting the equation of conservation as

$$\frac{Du_i}{Dt}=\frac{B_i}{\rho}-\frac{1}{\rho}\frac{\partial p_{ij}}{\partial x_j}, \quad (27)$$

and T_{ij}^* is defined in the same way as T_{ij} when ρ^* replaces ρ

3.2. Vascular sound field from a source point

For ease of analysis, but with no loss of generality, we conceive of a single point source in the arterial compartment as a source whose dimensions are much less than the wavelength of sound generated. The lengths of vascular vessels may be considered 'short'. Since details concerning turbulent fields in short vessels are sparse, the approximation of a random point source holds well. Assume $x_0 \in (l_1, l_2)$ is a source point in an arterial segment. We define the source point as

$$p_{turb}(\omega, x_0) = p_{turb}(\omega)\ell\,\delta(x-x_s)\ , \quad (28)$$

where p_{turb} is the turbulent pressure, ω the angle frequency, ℓ the effective length of the source, and x_s is the location of an equivalent source. The δ function here has units of L^{-1} (as in Succi [26]). The spatial Fourier expansion of the left-hand side of (28) gives

$$p_{turb}(\omega,\kappa_\pm)=\frac{1}{2\pi}\int_{-\infty}^{\infty}dx_0\,p_{turb}(\omega,x_0)e^{\mp i\kappa_\pm x_0} \quad (29)$$
$$=\frac{1}{2\pi}\int_{l_1}^{l_2}dx_0\,p_{turb}(\omega,x_0)e^{\mp i\kappa_\pm x_0}$$

where κ is the wave number. $\boldsymbol{l_1}$, is measured as the vessel's origin at the inception of turbulence, which may be numerically zero. It is assumed that the turbulent sources are contained completely inside the vessel and are sufficiently far from the ends. So, p_{turb} alongside the convective derivative dp_{turb}/dx_0 could be assumed zero at the inlet and exit. We situate the observation point outside the source region. The acoustic field of the point source reads:

$$p(\omega,l_1)=\frac{p_{turb}(\omega,l_1)i\pi\kappa\ell}{\ell(\omega,l_1)}\left\{\frac{1}{(1-M)^2}e^{i\kappa_- x_s}+\frac{1}{(1-M)^2}R_{l_2}e^{i(\kappa_++\kappa_-)l_2}e^{-i\kappa_+ x_s}\right\}, \quad (30)$$

where M is the Mach number, R_{l2} pressure reflection coefficient at pipe exit, l_2. The radiated field is

$$p(\omega,x)=\int_{l_1}^{l_2}p_{turb}(\omega,x_0)\left(\kappa-iM\frac{\partial}{\partial x_0}\right)^2 G_\omega(x\,|\,x_0), \quad (31)$$

where G denotes Green's function, which furnishes the linear acoustic response of a pipe and $G_\omega(x|x_0)$ denotes Green's function of the pressure field prompted by a harmonic source of unit strength located at $x = x_0$. The averaging over all source positions removes all dependence on x_s. Thus, from (30) we get

$$\left\langle |p(\omega,l_1)|^2 \right\rangle = \frac{1}{l_2}\int_{l_1}^{l_2} dx_s |p(\omega,l_1)|^2_{l_2} = \frac{|p_{turb}(\omega)|^2 \pi^2 \kappa^2 \ell^2}{|\ell(\omega)|^2}\left\{\frac{1}{(1-M)^4} + \frac{1}{(1-M)^4}|R_{l_2}|^2\right\} \quad (32)$$

Likewise, the average acoustic field of a distributed source over N measurements of incident pressure is

$$\left\langle |p(\omega,l_1)|^2 \right\rangle = \frac{1}{N}\sum_{n=1}^{N}|p(\omega,l_1)|_n^2 \quad (33)$$
$$= \frac{\pi^2\kappa^2}{|\ell(\omega)|^2}\left\{\frac{|p_{turb}(\omega,\kappa_-)|^2}{(1-M)^4} + \frac{|p_{turb}(\omega,\kappa_+)|^2}{(1-M)^4}R_{l_2}^{\ 2}\right\}.$$

3.3. Heart murmur

A heart murmur is propagated as compression and shear (elastic) waves. The heart may be conceived as an elastic spring due to its contractibility during systole and restitution during diastole. It is amenable to structural failure arising from the turbulent flow. Therefore, flow dampers may be used to mitigate the discomfort, damage, or structural failure resulting from the vibrating tissues. Heart motion may be modelled by using the general Hooke's law in conjunction with the Kelvin-Voigt viscoelastic model. Let us discuss, in passing, the Kelvin-Voigt model concerning the heart. (Kelvin-)Voigt model is denoted by a purely viscous damper and purely elastic spring connected in parallel as shown in Figure 1 below.

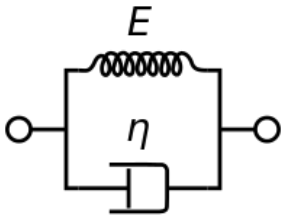

Figure 1. Schematic representation of the Kelvin-Voigt model [27]

The total stress will be the sum of the stress in viscous damper and purely elastic spring:

$$\sigma_{tot} = \sigma_S + \sigma_D. \quad (34)$$

where subscript S indicates the stress-strain in the spring and subscript D indicates the stress-strain in the damper. In a Kelvin-Voigt material, stress σ, strain ε and their time rates of change are governed by an equation of the form:

$$\sigma(t) = E\varepsilon(t) + \eta\frac{d\varepsilon(t)}{dt}, \quad (35)$$

Where, in (35) above, E is a modulus of elasticity and η is the viscosity.

If some constant stress σ_0 is suddenly applied to Kelvin-Voigt material, then the deformations would approach the deformation for the pure elastic material σ_0/E with the difference decaying exponentially. We get:

$$\varepsilon(t) = \frac{\sigma_0}{E}(1 - e^{-t/\tau R}), \quad (36)$$

where t is time and $\tau_R = \eta/E$ encodes the retardation time. The retardation at some time t_1 (when the material is freed) obeys the equation:

$$\varepsilon(t > t_1) = \varepsilon(t_1)e^{-(t-t_1)/\tau_R}. \qquad (37)$$

3.3.1. Murmur generation in the aorta

The governing equations of murmur concerning the Kelvin-Voigt model are (see Bailoor *et al.* [28]):

$$\frac{\partial p'_{ij}}{\partial t} + \lambda \frac{\partial u'_k}{\partial x_k}\delta_{ij} + \mu\left(\frac{\partial u'_i}{\partial x_j} + \frac{\partial u'_j}{\partial x_i}\right) = 0, \qquad (38\ a, b)$$

$$\rho_s \frac{\partial u'_i}{\partial t} + \frac{\partial p'_{ij}}{\partial x_j} = \nu \frac{\partial}{\partial x_j}\left(\frac{\partial u'_i}{\partial x_j} + \frac{\partial u'_j}{\partial x_i}\right)$$

where p'_{ij} and u'_i signify local elastic stress and velocity fluctuations, respectively. The adjoining organs, bones, blood volume, and other tissue are denoted by a homogenous medium with density ρ_s, Lamé parameters λ and μ, and viscosity ν. The propagation and dissipation of compressive (bulk) and shear waves within this homogenous viscoelastic medium are governed by equation (38*b*). The tissue-air interface on the epidermis is modelled as a traction-free surface and governing boundary condition read:

$$\begin{aligned} &p'_{ij}\boldsymbol{n}_j = 0 \\ &\left\{\lambda \frac{\partial u'_k}{\partial x_k}\delta_{ij} + \mu\left(\frac{\partial u'_i}{\partial x_j} + \frac{\partial u'_j}{\partial x_i}\right)\right\}\boldsymbol{n}_j = 0 \end{aligned}, \qquad (39)$$

where $\mathbf{n}_j$ encodes the surface normal. In elucidating the boundary condition on the aorta-surrounding tissue interface, Bailoor *et al.* [28] suggested that the viscous shear stress induced by blood flow may be presumed negligible relative to normal (pressure) forces. The consequential boundary condition reads:

$$\begin{aligned} &p'_{ij}\boldsymbol{n}_j = P'\boldsymbol{n}_i \\ &\left\{\lambda \frac{\partial u'_k}{\partial x_k}\delta_{ij} + \mu\left(\frac{\partial u'_i}{\partial x_j} + \frac{\partial u'_j}{\partial x_i}\right)\right\}\boldsymbol{n}_j = -\frac{\partial P'}{\partial t} \end{aligned}, \qquad (40)$$

where $P' = P - \bar{P}$ is the hemodynamic pressure fluctuation on the aorta lumen boundary. For the homogenous medium described above, the compression wave speed is given by $c_c = \sqrt{K/\rho_s}$, where $K = \lambda + 2\mu/3$ is the bulk modulus. Similarly, the shear wave speed is given by $c_s = \sqrt{\mu/\rho_s}$.

In the frequency domain, at low frequencies (<1000 Hz), the solution of equation (38) can be approximated by using the free space Green's tensor:

$$\mathcal{G}_{ij}(\mathbf{r},\omega) = \frac{ik_p}{12\pi(\lambda+2\mu)}[\delta_{ij}H_0^{(1)}(k_p r) + (\delta_{ij} - 3\frac{x_i x_j}{r^2})\Theta \qquad (41)$$

where

$$\Theta = H_n^{(1)}(k_p r)] - \frac{ik_s}{12\pi\mu}\left(-2\delta_{ij}H_0^{(1)}(k_s r)\right) + (\delta_{ij} - 3\frac{x_i x_j}{r^2})H_n^{(1)}(k_s r).$$

Mediterranean Journal of Basic and Applied Sciences (MJBAS)
Volume 7, Issue 1, Pages 154-166, January-March 2023

In (41) above:

$k_p = \omega/\sqrt{(\lambda+2\mu)/\rho_s}$ Encodes a longitudinal wavenumber,

$k_s = \omega/\sqrt{\mu/\rho_s}$ is the shear wavenumber,

$H^{(1)}{}_n$ is the spherical Hankel function of the first kind,

$x_{i\,j}$ is the vector from the source to the monitor point, with magnitude *r*.

The superposition principle gives the '*n*' component of surface acceleration at the monitor points on the aortic surface as

$$\boldsymbol{a}_n(\omega) = 2\sum_k (-i\omega)^2 \mathcal{G}_{nj}(\mathbf{r}_k, \omega) n_{j,k} \tilde{P}_k(\omega) \Delta A\,, \qquad (42)$$

where $\tilde{P}_k(\omega)$ indicates the hemodynamic pressure on the aorta lumen boundary in the frequency domain from the k^{th} element.

3.3.2. Sound signals and power

Turbulent sound signals may be estimated in numerous ways (see Akay *et al.* [1], Ahlström [29]), Qin [30]). Among the time-based characteristics are signal intensity and frequency. One may find the extensive work by Allen and Mills [31] on them quite invaluable. The continuous analytic signal consists of the original signal alongside its Hilbert transform given by [29, 27]:

$$s_{Analytic}(t) = s(t) + i.\frac{1}{\pi}\int_{-\infty}^{\infty}\frac{s(\tau)}{\tau - t}d\tau = s(t) + i.s_H(t)\,, \qquad (43)$$

where *H*(*t*) encodes the Hilbert transform. This signal has the following envelope:

$$_{env}s_{Analytic}(t) = \sqrt{|s(t)|^2 + |s_H(t)|^2}\,. \qquad (44)$$

The time-averaged frequency spectrum can be produced by using the Fourier transform. The windowed short-time Fourier transform (STFT) reads:

$$\mathcal{F}_{ST}(\zeta, k) = \sum_{t=1}^{N} s(t) w(t-\zeta) e^{-2\pi i \frac{kt}{N}}\,, \qquad (45)$$

where w represents the time window, ζ is the translation parameter and *k* the frequency parameter. Since for the STFT the frequency resolution decreases as the time resolution increases and vice versa, a better resolution is may be achieved by the use of shorter windows for higher frequencies and longer windows for lower frequencies. Thus, we employ the discrete wavelet transform (WT) furnished by Allen and Mills [31]:

$$WT(\zeta, \gamma) = \sum_{t=1}^{N} s(t) w\left(\frac{t-\zeta}{\gamma}\right) \qquad (46)$$

where γ is a scale parameter. The mother wavelet denoted w(*t*) may represent any signal that is decomposed into a series of dilatations or compressions. With the apparent loss of the link to local frequency by employing the wavelets the scaling term supplants the frequency.

Mediterranean Journal of Basic and Applied Sciences (MJBAS)
Volume 7, Issue 1, Pages 154-166, January-March 2023

On a continuous mode in the time domain, the wavelet transform takes the form:

$$W_s(t) = \gamma^{-1/2} \int_{-\infty}^{+\infty} s(t) w^*_{\gamma,\zeta} \left(\frac{t-\zeta}{\gamma} \right) dt \cdot \quad (47)$$

We have

$$W_s(t) = \int_{-\infty}^{+\infty} s(t) w^*_{\gamma,\zeta}(t) dt = \left\langle s(t), w_{\gamma,\zeta}(t) \right\rangle, \quad (48)$$

where the kernel function results from the scale parameter γ and time translation, ζ, of the window function. The wavelet transform in the frequency domain can as well be shown (see Qin [30]). The wavelet transforms method is crucial in converting the infinite trigonometric function basis in Fourier transform to a finite attenuated wavelet basis. It serves a dual purpose of furnishing both frequency and time. Wavelet analysis is an evolving trend in signal analysis.

4. Conclusions

Barring physiological circumstances as may be seen in some manoeuvres and other essences, stenosis is a culprit in turbulent cardiovascular flows. During systole, the blood immediately proximal to stenosis is known to undergo laminar flow. It only undergoes convective acceleration as it passes from the intact portion of the artery through the converging section of the stenosis. Turbulence occurs at a reasonably high Reynolds number and the flow through the diverging section of the stenosis splits from the walls on account of its inability to overcome the opposing pressure gradient. A shear layer predisposed to fluid-dynamical fluxes is created at the frontier between the separated high-velocity jet and the relatively slow-moving fluid in the recirculating separation zone. This shear layer that is created delivers a source from which these instabilities derive energy from the mean flow.

An arterial segment that is admitting a turbulent flow may be exposed to enormous fluctuating stresses. The vibrating structures, distressed regions of turbulent flow, mixing of flows of diverse temperatures, and their semblances induce large pressure fluctuations in the cardio-vascular system that are transferred through a fluid as sound. Studies revealed that turbulent blood flow generates sounds in partially occluded arteries in the event of coronary stenosis. Such pathological sounds are referred to as vascular bruits/murmurs. On this note, the salient details of this work are:

(a) The expression representing the sources that characterise the physical properties of the acoustic wave.

(b) The expression for the vascular sound field from a source point.

(c) The hemodynamic pressure fluctuation on the aorta lumen boundary and the consequential aortic (heart) murmur.

(d) The analysis of acoustic signals by the suitable transform method.

Interestingly, as may be deciphered from (d) above, acoustic quantities acquired from sensitive microphones placed on the chest are being used in a procedure for a non-invasive diagnosis of coronary artery disease. Moreover, the spectral content of isolated diastolic heart sounds/murmurs are being assessed by using exclusively developed signal processing techniques. The result indicates a rise in high-frequency components in patients with

occlusive coronary arteries. We adduce that Fourier and wavelet transform methods hold well for the analysis of sound signals emanating from cardiovascular sounds.

Declarations

Source of Funding

This research work did not receive any grant from funding agencies in the public or not-for-profit sectors.

Conflict of Interests

The authors declare the total absence of conflicts of interest, both during the conduct of the experiments and during the written drafting of this work.

Consent for Publication

The authors declare that they consented to the publication of this research work.

Acknowledgement

The authors are grateful to the reviewers for their attention to detail that helped in the revision of this paper.

References

[1] Y.M. Akay, M. Akay, W. Welkowitz, S. Lewkowicz, Y. Palti (1994). Dynamics of the Sounds Caused by Partially Occluded Femoral Arteries in Dogs. Annals of Biomedical Engineering, 22: 493–500.

[2] R. Lees and J. Kistler (1978). Carotid phonoangiography. In Noninvasive Diagnostic in Vascular Disease, A. Bernstein, Ed. St. Louis, MO: CV Mosby, Pages 187–194.

[3] Miller, R.S. Lees, J.P. Kistler, W.M. Abbott (1980). Spectral analysis of arterial bruits (phonoangiography): Experimental validation. Circulation, 63(3): 515–520.

[4] J-Z. Wang, B. Tie. W. Welkowitz, J.L. Semmlow, J.B. Kostis (1990). Modeling Sound Generation in Stenosed Coronary Arteries. IEEE Transactions on Biomedical Engineering, 37(2).

[5] J. Roffman and A. Fieldman (1980). Coronary by-pass-graft stenosis causing diastolic murmur in patient on hemodialysis. Chest, 78: 356–357.

[6] J.F. Sangster and C.M. Oakley (1973). Diastolic murmur of coronary artery stenosis, Brit. Heart, 35L:840–844.

[7] J. Semmlow, W. Welkowitz, J.B. Kostis, and J. Mackenzie (1983). Coronary artery disease correlates between diastolic auditory characteristics and coronary artery. IEEE Trans. Biomed. Eng., BME-30: 136–139.

[8] F.E. Nzerem (2022). Murmurs from the Vascular Members: A Generalized Theoretical Outlook. Asian Journal of Basic Science & Research, 4(4): 47–59.

[9] F.E. Nzerem and H.C. Ugorji (2022). Flow propensities in biological vessels and valves. International Journal of Mathematical Analysis and Modelling, 5(4): 175–187.

[10] F.E. Nzerem, H. C. Ugorji (2022). The Turbulent Lagrangian Dissipative Particle Velocity Statistics. Mediterranean Journal of Basic and Applied Sciences, 6(4): 84–92.

[11] A.S. Monin, A.M. Yaglom (1975). Statistical Fluid Mechanics, 1(1975). Mechanics of turbulence. MIT Press, Cambridge, MA.

[12] R.E. Klabunde (2021). Hemodynamics. In Cardiovascular Physiology Concepts, 3rd Ed., Wolters Kluwer Press. https://www.cvphysiology.com/Hemodynamics/H001.

[13] H.N. Sabbah, and P.D Stein (1976). Turbulent Blood Flow in humans, its primary role in the production of ejection murmurs. Circulation Research, 38(6): 513–522.

[14] J.J. Fredberg (1977). Origin and character of vascular murmurs: Model studies of the Acoustical Society of America, Pages 1077-1085. doi: 10.1121/1.381377.

[15] J.Y., David, S.A. Jones, D.P. Giddens (1991). Modern spectral analysis techniques for blood flow velocity and spectral measurements with pulsed doppler ultrasound. IEEE Trans. Biomed. Eng., 38(1991): 589–596.

[16] J. Laufer, The structure of turbulence in fully developed pipe flow, Report 1174, naca.central.cranfield.ac.uk› reports ›naca-report-1174.

[17] A.D. Pierce (1991). Acoustics: An introduction to its physical principles and applications. The Acoustical Society of America.

[18] M. Carley, Turbulence and noise. https://people.bath.ac.uk.

[19] C.L. Morfey and M.CM. Wright (2007). Extension of Lighthill's acoustic analogy with application to computational aeroacoustics. Proc. R. Soc. A., 463: 2101–2127. doi: 10.1098/ rspa.2007.1864.

[20] F.C. Johansen (1929). Flow Through Pipe Orifices at Low Reynolds Number. Phys. H. Sec., Lend. Set. A., 126: 231–245.

[21] C. Gotia and N.A. Evans (1973). Flow Separation Through Annular Constrictions in Tubes. Exp. Mech., L3: 157-162.

[22] J.E. Ffowcs Williams, & D.L. Hawkings (1969). Sound generation by turbulence and surfaces in arbitrary motion. Phil. Trans. R. Soc. A., 264: 321–342. doi: 10.1098/rsta.1969.0031.

[23] M.J. Lighthill (1952). On Sound Generated Aerodynamically, I. General Theory, Proc. Roy. Soc. London, A 211: 564–587.

[24] G. Reethuf (1978). Turbulence-generated noise in pipe flow. Ann. Rev. Fluid Mech., 10: 333–67.

[25] R.S. Reneman, van Merode, T., Hick, P., Muytjens, A.M., Hoeks, A.P. (1986). Age-related changes in carotid artery wall properties in men. Ultrasound Med Biol., 12: 465–471.

[26] G.P. Succi (1977). The interaction of sound with turbulent flow. Ph.D Thesis.cn--Massachusetts Institute of Technology, Dept. of Physics, http://hdl.handle.net/1721.1/27891 (Accessed: March 15, 2022).

[27] Kelvin–Voigt material, https://en.wikipedia.org/w/index.php?title=_Kelvin%E2%80%93Voigt_material&oldid=1136082879 (Assessed: March 20, 2023).

[28] S. Bailoor, J-H. Seo, S. Schena, R. Mittal, Detecting aortic valve anomaly from induced murmurs: insights from computational hemodynamic models, Front. Physiol., doi: https://doi.org/10.3389/fphys.2021.734224.

[29] C. Ahlström, Processing of the Phonocardiographic Signal−Methods for the Intelligent Stethoscope. http://www.diva-portal.org/smash/get/diva2:22548/FULLTEXT01.pdf (Assessed: March 20, 2023).

[30] W. Qin (2022). Signal Analysis of Characteristics Using Passive Acoustic Emission Technique in Gas-Solid Pipeline Flows. Discrete Dynamics in Nature and Society, Pages.1-7. doi: https://doi.org/10.1155/2022/7848008.

[31] R.L. Allen and D.W. Mills (2004). Signal analysis: time, frequency, scale and structure. New York, Piscataway, N.J. Wiley, IEEE Press.